Flow Turbulence Combust (2012) 89:449–464
DOI 10.1007/s10494-012-9399-7

Large-Eddy Simulation of a Jet-in-Hot-Coflow Burner Operating in the Oxygen-Diluted Combustion Regime

Matthias Ihme · Jian Zhang · Guowei He · Bassam Dally

Received: 5 October 2011 / Accepted: 8 May 2012 / Published online: 26 May 2012

Abstract Large-eddy simulations of moderate and intense low-oxygen dilution (MILD) combustion of a jet-in-hot-coflow (JHC) burner are performed. This burner configuration consists of three streams, providing fuel, oxygen-diluted coflow, and air to the burner. To account for the mixing between the three reactant streams, a three-stream flamelet/progress variable (FPV) formulation is utilized. This model was previously applied to a condition corresponding to the upper range of MILD-combustion, and the objective of this contribution is to further investigate this model in application to highly diluted operating conditions. Comparisons of mean and conditional results show that the model accurately captures effects of increasing oxygen-depletion on the flame-structure and heat-release, and predictions for temperature and species mass fractions are in overall good agreement with experiments.

Keywords MILD combustion · Flamelet modeling · Turbulent non-premixed flames · Large-eddy simulation · Three-stream combustion

1 Introduction

Combustion technologies, referred to as moderate and intense low-oxygen dilution (MILD), are attractive alternatives to conventional combustion systems for improving the thermal efficiency and for reducing pollutant emissions [1]. In these

M. Ihme (✉) · J. Zhang
Department of Aerospace, University of Michigan, Ann Arbor, MI 48109, USA
e-mail: mihme@umich.edu

J. Zhang · G. He
LNM, Institute of Mechanics, Chinese Academy of Sciences, Beijing, 100190, China

B. Dally
School of Mechanical Engineering, The University of Adelaide,
South Australia 5005, Australia

technologies the reactant mixture is preheated by hot reaction products. In addition, the lower oxygen concentration leads to reduction in the flame temperature, thereby decreasing pollutant emissions such as soot and nitrogen oxide.

MILD combustion, which is also referred to as flameless oxidation (FLOX) [2], colorless combustion [3], or high-temperature air combustion (HiTAC) [4], is commonly defined as a combustion process in which the reactant temperature exceeds the autoignition temperature of the mixture, and the temperature increase due to heat release does not exceed the self-ignition temperature [1]. In the context of non-premixed combustion regimes, Oberlack et al. [5] associated MILD-combustion with the condition in which the quenching and ignition points collapse and the combustion process continuously shifts between unburned and burned conditions.

To achieve the required preheat temperature in MILD combustion, product gases are mixed with reactants. In practical systems this is typically accomplished by means of recuperation or internal recirculation. Due to the significant dilution of the reactants with product gases, the chemical reactivity of the mixture is reduced, so that the combustion process is primarily controlled by chemical-kinetics processes. To quantify this effect, a Damköhler number can be introduced, comparing the characteristic convective time scale to the chemical time scale:

$$\mathrm{Da} = \frac{\tau_{\mathrm{flow}}}{\tau_{\mathrm{chem}}} = \frac{D_{\mathrm{ref}}}{U_{\mathrm{ref}}} \frac{\dot{\omega}^*_{C,\mathrm{st}}}{C^*_{\mathrm{st}}} \,. \tag{1}$$

In this equation, D_{ref} and U_{ref} are the reference length scale and velocity of the burner and the chemical time-scale is defined from the stoichiometric value of the progress variable, C^*_{st} that is evaluated at its maximum production rate, $\dot{\omega}^*_{C,\mathrm{st}}$, occurring near the quenching—or inflection-point—condition along the flamelet S-shape curve (see symbols in Fig. 3).

Over recent years, several experimental studies have been conducted to investigate MILD combustion. Plessing et al. [6] performed measurements in a confined combustor that was operated with preheated air and significant exhaust gas recirculation. They found that the strong flame stretching due to high flow velocities leads to disconnected reaction zones. Flameless combustion was only achieved if the temperature of the unburned mixture exceeded 950K, and the maximum flame temperature in the combustor did not exceed 1650K. Dally et al. [7] developed a three-stream jet-in-hot-coflow (JHC) burner in which the coflow was generated by mixing hot reaction products with oxygen and nitrogen. By systematically varying the oxygen-concentration between 9, 6, and 3%, they performed detailed measurements to investigate effects of decreasing oxygen levels on the flame structure. In decreasing order of oxygen-concentration, these three flames are denoted by HM3, HM2, and HM1, respectively.

Recently, Oldenhof et al. [8, 9] conducted scalar and velocity measurements in a modified JHC-burner to characterize lift-off behavior and coupling effects between turbulence and chemistry in the MILD combustion regime. Supported by theoretical analysis, their experimental investigations showed that the ignition location and flame-stabilization in this burner is controlled by the entrainment of oxidizer from the hotter region in the coflow. These findings further illustrate the sensitivity of the ignition-mechanisms under MILD-operating conditions.

Numerical investigations of MILD combustion have largely relied on Reynolds-averaged Navier-Stokes (RANS) formulations. Coelho and Peters [10] applied an

Eulerian particle flamelet model to predict the nitric oxide (NO) formation in a FLOX-burner that was experimentally studied by Plessing et al. [6]. They showed that the unsteady formulation is able to capture the NO-emission under MILD combustion conditions. Christo and Dally [11] conducted RANS-studies of a JHC burner in order to assess the performance of various turbulence models, chemical mechanisms and combustion models, including the steady flamelet model, the eddy dissipation concept (EDC), and a transported probability density function (PDF) model. By considering the same experimental configuration, Kim et al. [12] used a conditional moment closure (CMC) model to predict the flame structure and NO formation. The EDC-model was also utilized by De et al. [13] to investigate its performance in combination with a two-equation turbulence model and reduced methane/air mechanisms. They showed that, although the model overpredicts the onset of ignition, it accurately captured the sensitivity of the lift-off height with respect to Reynolds number.

In contrast to the single-mixture fraction formulation, employed in [11], Ihme and See [14] proposed a flamelet-model for application to three-stream combustion systems. In this three-stream flamelet/progress variable (FPV) model, the oxidizer split was introduced as an additional scalar to predict the mixing between two oxidizer streams and the fuel stream. The model was successfully applied in LES of the HM3 configuration of the JHC-burner of Dally et al. [7], and the sensitivity of the flame-structure to variations in scalar inflow conditions were studied. By complementing this investigation, the objective of this paper is to apply the three-stream FPV combustion model to increasingly more complex combustion conditions that are reflected by higher oxygen dilution levels. To this end, LES computations of three different operating conditions are performed, in which the nominal oxygen mass fraction in the coflow stream is continuously reduced from 9% to 6%, and eventually down to 3%. Experimental data are used to assess the performance and accuracy of this three-stream LES combustion model.

The remainder of this paper is organized as follows. The mathematical model and experimental configuration are presented in Sections 2 and 3, respectively. Simulation results and comparisons with experimental data are presented in Section 4, and the paper finishes with conclusions.

2 Mathematical Model

In the present study, a three-stream LES combustion model is used to simulate a series of flames that are operated in a JHC burner. A schematic of the burner is shown in Fig. 1. In this burner, fuel is supplied through a central nozzle, which is surrounded by a coflow, and shroud air enters the burner through the outermost stream. Since the coflow and the shroud air both provide oxidizer to the flame, we will refer to both streams collectively as oxidizer-stream. The lower part of the flame is established through the reaction between the diluted hot coflow and the central fuel stream. With increasing downstream distance, shroud air is entrained into the core-region, displacing the coflow. This leads to the reaction of the excess fuel with oxygen-rich shroud air in the upper part of the flame.

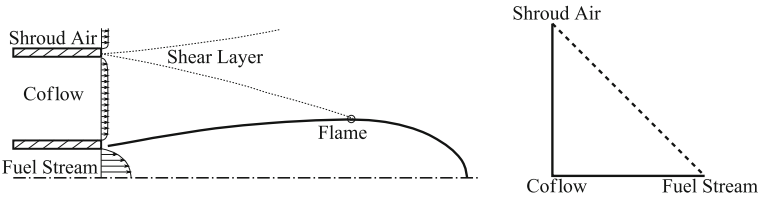

Fig. 1 Schematic of the JHC burner configuration

The one-dimensional flame structure in the three-stream burner system is described from the solution of the steady flamelet equations:

$$-\frac{\chi_Z}{2}\frac{\partial^2 \boldsymbol{\phi}}{\partial Z^2} = \dot{\boldsymbol{\omega}} \,, \tag{2}$$

where Z is the mixture fraction, $\boldsymbol{\phi}$ is the vector of all species mass fractions $\boldsymbol{Y}$ and temperature T, and $\dot{\boldsymbol{\omega}}$ denotes their respective source terms. The scalar dissipation rate is denoted by χ_Z with $\chi_Z = 2\alpha|\nabla Z|^2$, and α is the molecular diffusivity. Preferential diffusion effects are not considered in Eq. 2.

Boundary conditions are provided by specifying the composition in the oxidizer stream ($Z = 0$, superscript "O") and in the fuel stream ($Z = 1$, superscript "F"):

$$\boldsymbol{\phi}(Z = 0) = \boldsymbol{\phi}^{\mathrm{O}} \,, \tag{3a}$$

$$\boldsymbol{\phi}(Z = 1) = \boldsymbol{\phi}^{\mathrm{F}} \,. \tag{3b}$$

To account for mixture variations in the oxidizer stream, corresponding to the coflow, shroud air stream, and respective intermediate compositions, the mixture composition at $Z = 0$ is expressed in terms of the oxidizer split W. In the following, the dependence of the oxidizer composition is explicitly denoted by the superscript "O(W)." The resulting expression for the oxidizer composition can then be written as:

$$\boldsymbol{\phi}(Z = 0) = \boldsymbol{\phi}^{\mathrm{O}(W)} \,, \tag{4}$$

and $\boldsymbol{\phi}^{\mathrm{O}(W)}$ can be obtained from the solution of a scalar mixing problem between the coflow and the shroud air stream. The oxidizer split is assigned to be zero in the coflow and unity in the shroud air stream.

The mixture fraction and oxidizer split can be related to the elemental species mass fractions through the following expression:

$$\begin{pmatrix} Z \\ W \end{pmatrix} = \underline{\underline{A}}^{-1} \begin{pmatrix} y_{\mathrm{C}} - y_{\mathrm{C}}^{\mathrm{O}(0)} \\ y_{\mathrm{O}} - y_{\mathrm{O}}^{\mathrm{O}(0)} \end{pmatrix} \quad \text{with} \quad \underline{\underline{A}} = \begin{pmatrix} y_{\mathrm{C}}^{\mathrm{F}} - y_{\mathrm{C}}^{\mathrm{O}(0)} & -y_{\mathrm{C}}^{\mathrm{O}(0)} \\ -y_{\mathrm{O}}^{\mathrm{O}(0)} & y_{\mathrm{O}}^{\mathrm{O}(1)} - y_{\mathrm{O}}^{\mathrm{O}(0)} \end{pmatrix} \,, \tag{5}$$

where the superscripts "O(0)" and "O(1)" refer to the coflow ($W = 0$) and the shroud air stream ($W = 1$), and the elemental mass fractions of carbon and oxygen are denoted by y_{C} and y_{O}, respectively. In the absence of oxygen in the fuel-stream, the elemental mass fraction of oxygen can be expressed in terms of the mixture fraction and the elemental oxygen-mass fraction in the oxidizer stream $y_{\mathrm{O}}^{\mathrm{O}(W)}$:

$$y_{\mathrm{O}} = y_{\mathrm{O}}^{\mathrm{O}(W)}(1 - Z) \,. \tag{6}$$

With this, the expression for the oxidizer split from Eq. 5 can be written as:

$$W = (1 - Z) \left(\frac{y_{\mathrm{O}}^{\mathrm{O}(0)} - y_{\mathrm{O}}^{\mathrm{O}(W)}}{y_{\mathrm{O}}^{\mathrm{O}(0)} - y_{\mathrm{O}}^{\mathrm{O}(1)}} \right) . \tag{7}$$

Recognizing that the multiplicand in this expression is independent of Z, a mixture-fraction independent variable can be defined as:

$$\mathcal{W} = \frac{W}{1 - Z} \qquad \text{with} \qquad \mathcal{W} = \frac{y_{\mathrm{O}}^{\mathrm{O}(0)} - y_{\mathrm{O}}^{\mathrm{O}(W)}}{y_{\mathrm{O}}^{\mathrm{O}(0)} - y_{\mathrm{O}}^{\mathrm{O}(1)}} . \tag{8}$$

In the following, we will refer to $\mathcal{W}$ as modified oxidizer split. Note that $\mathcal{W}$ is constant for each flamelet, and the value of $\mathcal{W}$ is evaluated from the elemental oxygen mass fraction on the oxidizer side.

The transport equations for the evolution of Z and $\mathcal{W}$ can be written as:

$$\rho \mathcal{D}_t Z = \nabla \cdot (\rho \alpha \nabla Z) , \tag{9a}$$

$$\rho \mathcal{D}_t \mathcal{W} = \nabla \cdot (\rho \alpha \nabla \mathcal{W}) - \frac{2}{1 - Z} \rho \alpha \nabla \mathcal{W} \cdot \nabla Z , \tag{9b}$$

where $\mathcal{D}_t = \partial_t + \boldsymbol{u} \cdot \nabla$ is the substantial derivative, and the last term on the right-hand-side of Eq. 9b represents a cross-dissipation term. The solution of the flamelet equations under consideration of compositional variations in the oxidizer stream can then be written as:

$$\boldsymbol{\phi} = \boldsymbol{\phi}(Z, \mathcal{W}, \chi_{Z,\mathrm{st}}) , \tag{10}$$

where $\chi_{Z,\mathrm{st}}$ is the stoichiometric mixture fraction, which is related to χ_Z. As an example, the solution of this three-stream flamelet-formulation is illustrated in Fig. 2, showing the temperature and the CO mass fraction as function of Z and $\mathcal{W}$. These flamelets are evaluated for a constant stoichiometric scalar dissipate rate of $\chi_{Z,\mathrm{st}} = 10\ \mathrm{s}^{-1}$. The composition for the fuel and oxidizer streams corresponds to the HM3 operating condition [7], and is summarized in Table 2. This figure shows that with increasing oxidizer split (corresponding to increasing oxygen concentration), the maximum flame temperature increases by approximately 250K and the value for the stoichiometric mixture fraction shifts towards richer mixtures.

In the context of the FPV model, a reaction progress variable C was introduced to eliminate the explicit dependence of the thermochemical quantities on the scalar dissipation rate in the steady flamelet library [15]. This transformation provides a unique representation of all thermochemical quantities over the entire solution space of the steady flamelet equations. With this, the FPV library for a three-stream combustion system can be written as:

$$\boldsymbol{\phi} = \boldsymbol{\phi}(Z, \mathcal{W}, C) , \tag{11}$$

where the reaction progress variable is defined as a linear combination of major species: $C = Y_{\mathrm{CO_2}} + Y_{\mathrm{CO}} + Y_{\mathrm{H_2O}} + Y_{\mathrm{H_2}}$.

For application of the three-stream FPV combustion model to LES, the Favre-filtered quantities are obtained by integrating Eq. 11 over the joint probability density function (PDF), $\widetilde{P}(Z, \mathcal{W}, C)$, where the tilde denotes a Favre-averaged quantity. Since Z and $\mathcal{W}$ are independent, the joint PDF can be written as

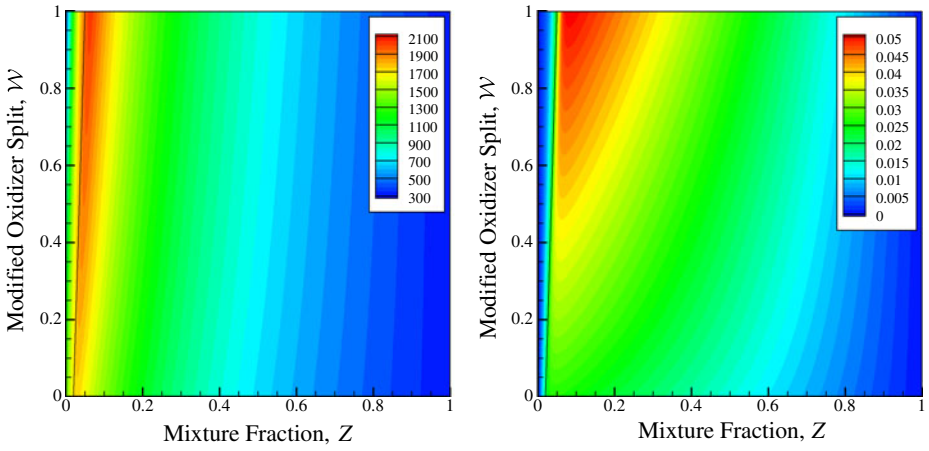

(a) Temperature. (b) CO Mass Fraction.

Fig. 2 Flamelet solution for a three-stream combustion system, showing **a** temperature T and **b** CO mass fraction as function of mixture fraction Z and modified oxidizer split $\mathcal{W}$, evaluated at a constant stoichiometric scalar dissipate rate of $\chi_{Z,\mathrm{st}} = 10\ \mathrm{s}^{-1}$. The mixture composition corresponds to the HM3 flame configuration [7], which is summarized in Table 2. The *solid lines* indicate the location of the stoichiometric mixture fraction Z_{st}

$\widetilde{P}(Z)P(\mathcal{W})P(C|Z,\mathcal{W})$. The marginal PDFs for mixture fraction and modified oxidizer split are described by a presumed beta-PDF, and the conditional PDF of the reaction progress variable is modeled as a Dirac-delta function. With this, the Favre-averaged library of the FPV model can then be parameterized as:

$$\widetilde{\boldsymbol{\phi}} = \widetilde{\boldsymbol{\phi}}\left(\widetilde{Z}, \widetilde{Z''^2}, \widetilde{\mathcal{W}}, \widetilde{\mathcal{W}''^2}, \widetilde{C}\right). \tag{12}$$

In addition to the solution of the conservation equations for mass and momentum, the low-Mach number, variable-density LES-formulation requires the solution of five additional transport equations for the first two moments of mixture fraction and modified oxidizer split, and the mean progress variable. These modeled equations take the following form:

$$\overline{\rho}\widetilde{\mathcal{D}}_t\widetilde{Z} = \nabla\cdot\left(\overline{\rho}\widetilde{\alpha}\nabla\widetilde{Z}\right) + \nabla\cdot\boldsymbol{\tau}^{\mathrm{res}}_{\widetilde{Z}}\,, \tag{13a}$$

$$\overline{\rho}\widetilde{\mathcal{D}}_t\widetilde{Z''^2} = \nabla\cdot\left(\overline{\rho}\widetilde{\alpha}\nabla\widetilde{Z''^2}\right) + \nabla\cdot\boldsymbol{\tau}^{\mathrm{res}}_{\widetilde{Z''^2}} - 2\overline{\rho}\widetilde{\boldsymbol{u}''Z''}\cdot\nabla\widetilde{Z} - \overline{\rho}\widetilde{\chi}^{\mathrm{res}}_{Z}\,, \tag{13b}$$

$$\overline{\rho}\widetilde{\mathcal{D}}_t\widetilde{\mathcal{W}} = \nabla\cdot\left(\overline{\rho}\widetilde{\alpha}\nabla\widetilde{\mathcal{W}}\right) + \nabla\cdot\boldsymbol{\tau}^{\mathrm{res}}_{\widetilde{\mathcal{W}}} - \frac{2}{1-\widetilde{Z}}\overline{\rho}\widetilde{\alpha}\nabla\widetilde{\mathcal{W}}\cdot\nabla\widetilde{Z}\,, \tag{13c}$$

$$\begin{aligned}\overline{\rho}\widetilde{\mathcal{D}}_t\widetilde{\mathcal{W}''^2} = {}& \nabla\cdot\left(\overline{\rho}\widetilde{\alpha}\nabla\widetilde{\mathcal{W}''^2}\right) + \nabla\cdot\boldsymbol{\tau}^{\mathrm{res}}_{\widetilde{\mathcal{W}''^2}} - 2\overline{\rho}\widetilde{\boldsymbol{u}''\mathcal{W}''}\cdot\nabla\widetilde{\mathcal{W}} - \overline{\rho}\widetilde{\chi}^{\mathrm{res}}_{\mathcal{W}} \\ & - \frac{2}{1-\widetilde{Z}}\overline{\rho}\widetilde{\alpha}\nabla\widetilde{\mathcal{W}}\cdot\nabla\widetilde{Z''^2}\,,\end{aligned} \tag{13d}$$

$$\overline{\rho}\widetilde{\mathcal{D}}_t\widetilde{C} = \nabla\cdot\left(\overline{\rho}\widetilde{\alpha}\nabla\widetilde{C}\right) + \nabla\cdot\boldsymbol{\tau}^{\mathrm{res}}_{\widetilde{C}} + \overline{\rho}\widetilde{\dot{\omega}}_C\,, \tag{13e}$$

in which the turbulent fluxes are modeled by a gradient transport assumption [16], and the residual scalar dissipation rates $\widetilde{\chi}_Z^{\mathrm{res}}$ and $\widetilde{\chi}_{\mathcal{W}}^{\mathrm{res}}$ are modeled using spectral arguments [17]. Closure for the transport equations of $\widetilde{\mathcal{W}}$ and $\widetilde{\mathcal{W}''^2}$ is obtained by expanding the term $(1-Z)^{-1}$ to first order, and by invoking statistical independence so that all subgrid cross-dissipation terms and cross-correlations are neglected.

3 Experimental Configuration and Numerical Setup

3.1 Experimental setup

The three-stream FPV combustion model is applied to LES of the JHC burner that was experimentally studied by Dally et al. [7]. A schematic of the burner is illustrated in Fig. 1. The burner consists of a central jet, supplying a methane/hydrogen mixture in the ratio of 1:2 by volume. The diameter of the fuel pipe is $D_{\mathrm{ref}} = 4.25$ mm and the bulk exit velocity is $U_{\mathrm{ref}} = 73.5$ m/s, corresponding to a jet exit Reynolds number of 9500. The central jet is surrounded by a coflow. The coflow is generated by a secondary burner, providing hot combustion products to which oxygen and nitrogen are mixed in order to obtain a specified overall oxygen-concentration. The outer diameter of the coflow annulus is 82 mm, and the reported mass flow rate is 4.8 g/s. The burner is mounted in a wind tunnel, supplying shroud air at ambient condition at a velocity of 3.2 m/s.

A series of experiments were conducted to investigate effects of oxygen dilution on the flame structure. For this, the oxygen-mass fraction in the coflow was successively reduced in three steps while increasing the amount of N_2 to keep the hot coflow temperature constant. In increasing order of oxygen mass fraction in the coflow, these three operating conditions are designated as HM1 (3%), HM2 (6%), and HM3 (9%). For completeness, the operating conditions and experimental parameters are summarized in Tables 1 and 2. The Damköhler numbers are evaluated using Eq. 1 and are given in the third column of Table 2, showing that the characteristic Damköhler number changes by more than an order of magnitude between the three flames. For reference, the Damköhler number for a standard flame, which is operated with ambient air and the same fuel-composition, is Da = 1.45—three times larger than that of the HM3-flame.

A comparison of the calculated S-shaped curves for the three flames is presented in Fig. 3. This figure shows that with decreasing oxygen mass fraction in the coflow the peak stoichiometric flame temperature decreases by approximately 450K, and

Table 1 Global reference parameters for the JHC simulations [7]

Parameter	Fuel	Coflow	Shroud air
d [mm]	4.25 ($\equiv D_{\mathrm{ref}}$)	82	250
U [m/s]	73.5 ($\equiv U_{\mathrm{ref}}$)	3.2	3.2
Re	9500	1200	49700
T [K]	305	1300	300
$\widetilde{Z}/\widetilde{Z''^2}$	1/0	0/0	0/0
$\widetilde{\mathcal{W}}/\widetilde{\mathcal{W}''^2}$	0/0	0*/0	1/0
$\widetilde{C}$	0.2	0.12*	0

Values, denoted by an asterisk, denote nominal quantities

Table 2 Flame characteristics and mixture composition of the coflow for the three operating conditions of the JHC burner [7]

Case	Z_{st}	Da	Coflow $Y_{O_2}/Y_{N_2}/Y_{H_2O}/Y_{CO_2}$ [%]
HM3	0.0184	4.76×10^{-1}	9/79/6.5/5.5
HM2	0.0123	1.74×10^{-1}	6/82/6.5/5.5
HM1	0.0062	2.80×10^{-2}	3/85/6.5/5.5

The mixture composition in the coflow stream corresponds to the nominal operating condition, assuming homogeneous inflow composition. The composition of the fuel stream is $Y_{CH_4}/Y_{H_2} = 0.8/0.2$ and the composition of the shroud air stream is $Y_{O_2}/Y_{N_2} = 0.233/0.767$

the transition point between burned and unburned condition decreases by two orders of magnitude. For reference, the S-shape curve of a standard flame is shown by the dotted line, illustrating the distinct quenching point and higher flame temperature compared to the MILD combustion regime.

3.2 Numerical setup

The Favre-filtered governing equations are solved in cylindrical coordinates $(x, r, \theta)^T$. The non-dimensionalized computational domain is $40D_{ref} \times 20D_{ref} \times 2\pi$ in axial, radial, and azimuthal direction, respectively. The domain is discretized by a mesh of $192 \times 165 \times 64$ control volumes in axial, radial, and azimuthal directions, respectively. The minimum and maximum filter widths are $\Delta_{min} = 1.5 \times 10^{-2} D_{ref}$ (nozzle exit) and $\Delta_{max} = 7.5 \times 10^{-1} D_{ref}$ (exit plane).

Steady flamelet calculations were performed using the FlameMaster code [18] and the GRI 2.11 mechanism [19]. The Favre-filtered FPV chemistry library is parameterized in terms of $\widetilde{Z}$, $\widetilde{S}_Z = \widetilde{Z''^2}/(\widetilde{Z} - \widetilde{Z}^2)$, $\widetilde{\mathcal{W}}$, and $\widetilde{S}_{\mathcal{W}} = \widetilde{\mathcal{W}''^2}/(\widetilde{\mathcal{W}} - \widetilde{\mathcal{W}}^2)$.

3.3 Specification of inflow boundary conditions

The inflow velocity profile in the fuel-stream is prescribed from the solution of a turbulent periodic pipe-flow simulation by enforcing the experimentally reported

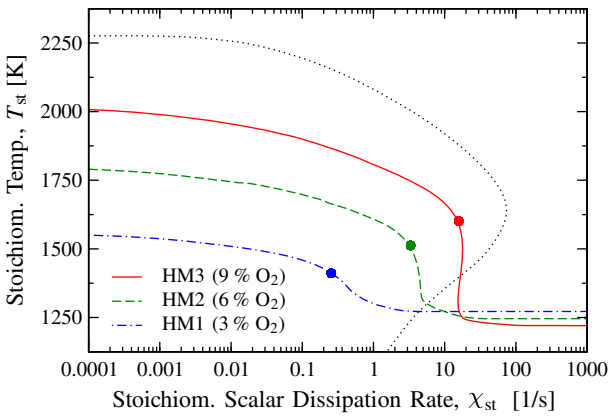

Fig. 3 Comparison of calculated S-shape curves for different levels of oxygen-mass fraction in fuel stream; see Table 2 for mixture composition. For reference, the *dotted black line* shows the S-shape curve for a diffusion flame, in which the coflow mixture is replaced by air at ambient condition. The symbols indicate the conditions at which the chemical time-scale in Eq. 1 was evaluated

bulk flow velocity. Velocity profiles in the coflow and air stream were prescribed by a laminar shear-layer profile:

$$\widetilde{u}(r) = \mathcal{U} \tanh\left(\frac{1}{\delta}\frac{r - R_\mathrm{i}}{R_\mathrm{o} - R_\mathrm{i}}\right) \tanh\left(\frac{1}{\delta}\frac{r - R_\mathrm{o}}{R_\mathrm{i} - R_\mathrm{o}}\right), \tag{14}$$

where $\widetilde{u}$ is the Favre-filtered axial velocity component, the parameter δ controls the shear layer thickness and is set to 0.1 for both streams. The coefficient $\mathcal{U}$ is adjusted to match the reported bulk flow rates in the coflow and in the outer stream, and R_i and R_o are the inner and outer radii of the annulus, respectively.

For the three-stream FPV model, boundary conditions for the five independent scalar quantities at the inflow-streams must be provided. Since the composition in the fuel and shroud air streams are homogeneous, constant values for the mean quantities and zero-variance are specified (see Table 1). However, the composition in the coflow is generated from a secondary burner, resulting in a spatially inhomogeneous distribution of scalar and temperature conditions. Therefore, a set of scalar inflow-conditions for $\widetilde{Z}, \widetilde{\mathcal{W}}$, and $\widetilde{C}$ is required to accurately represent the temperature and mixture composition at the coflow exit plane. In the present work, these scalar boundary conditions are obtained as a result of an optimization problem. To this end, measurements of scatter data in the coflow along the cross-sectional plane at $x/D_\mathrm{ref} = 0.94$ are used to constrain the scalar inflow conditions. First, exit conditions for the progress variable are directly evaluated from the experimental data:

$$\widetilde{C}(r) = \frac{1}{N}\sum_{i=1}^{N}\left(Y^{\mathrm{exp}}_{\mathrm{CO_2},i}(r) + Y^{\mathrm{exp}}_{\mathrm{CO},i}(r) + Y^{\mathrm{exp}}_{\mathrm{H_2O},i}(r) + Y^{\mathrm{exp}}_{\mathrm{H_2},i}(r)\right), \tag{15}$$

where $Y^{\mathrm{exp}}_{\phi,i}(r)$ denotes the i^{th} single-point measurement of species ϕ at the radial location r. Boundary conditions for the mean mixture fraction are assigned to be zero in the coflow. With these conditions for $\widetilde{C}$ and $\widetilde{Z}$, boundary conditions for $\widetilde{\mathcal{W}}$ are determined by minimizing the least-square error between single-point measurements and the FPV flamelet table (Eq. 12):

$$\min_{\widetilde{\mathcal{W}}(r)} \quad \sum_i \left[\boldsymbol{\phi}_i^{\mathrm{exp}}(r) - \widetilde{\boldsymbol{\phi}}\left(\widetilde{Z}(r), 0, \widetilde{\mathcal{W}}(r), 0, \widetilde{C}(r)\right)\right]^2. \tag{16}$$

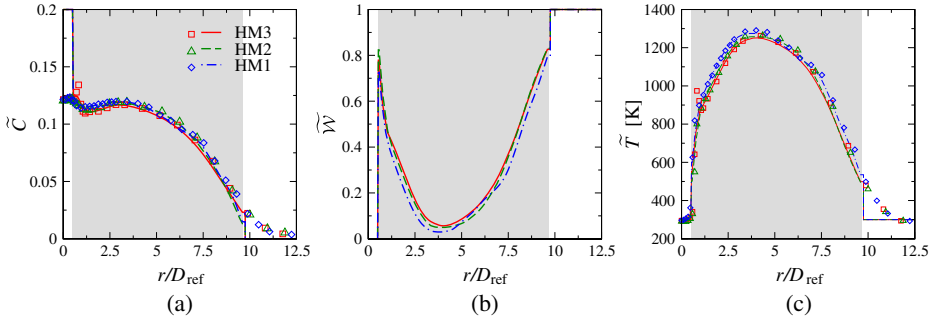

Fig. 4 Prescribed inflow boundary conditions for **a** progress variable, **b** modified oxidizer split, and **c** resulting temperature evaluated from the three-stream FPV chemistry library. The *gray area* indicates the region of the coflow-stream

Only mean-flow quantities are specified at the inflow, and fluctuations in the scalar boundary conditions are not considered in this investigation.

The evaluated inflow-boundary conditions for progress variable and oxidizer split are shown in Fig. 4a and b. The corresponding radial temperature profiles for all three operating conditions are presented in Fig. 4c. It is noted that the inflow conditions are evaluated from the measurements at 4 mm above the burner exit. It will be shown in the next section that the flow-structure within the first nozzle-diameter downstream of the exit is fairly constant, so that this procedure of providing inflow conditions appears to be adequate.

4 Results and Discussions

In this section, results from the three LES calculations are presented and compared with experimental data [7]. We first provide a qualitative comparison of the temperature field for the three flame configurations. This is followed by a quantitative analysis of temperature and species profiles in physical and mixture fraction space.

A comparison of the mean temperature fields of the three flames is shown in Fig. 5. The dashed lines indicate the stoichiometric contour and the solid lines correspond to the temperature isocontour of $T = 1350$K. From this figure, the effect of decreasing oxygen level on the flame temperature can be qualitatively observed. Specifically, with decreasing oxygen-concentration the flame temperature decreases, and the flame-base, which is here associated with the temperature isocontour of 1350K, moves further away from the nozzle. It can also be seen that the location of maximum temperature is located on the fuel-rich side of the flame. Figure 5 also shows that

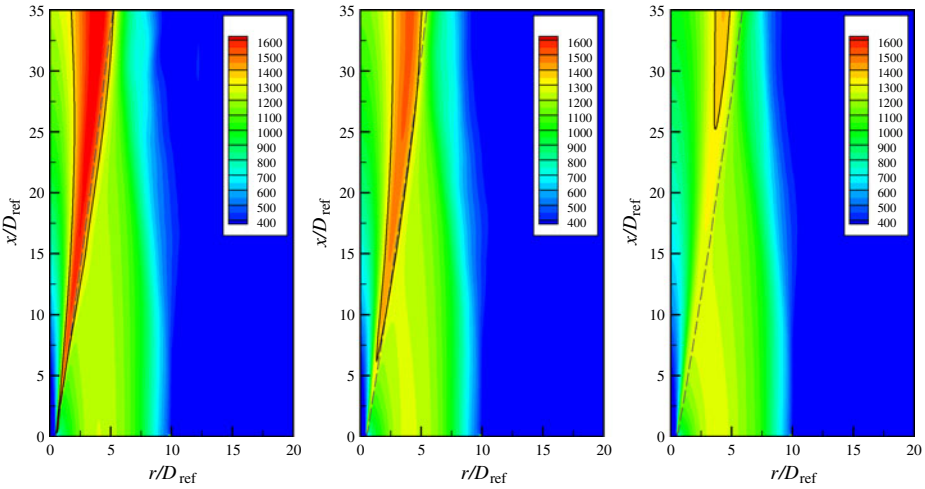

(a) HM3 (9% O_2) (b) HM2 (6% O_2) (c) HM1 (3% O_2)

Fig. 5 Mean temperature fields obtained from the LES calculations for all three flames. The *dashed lines* indicate the stoichiometric contour and the *solid lines* correspond to the temperature isocontour of $T = 1350$K

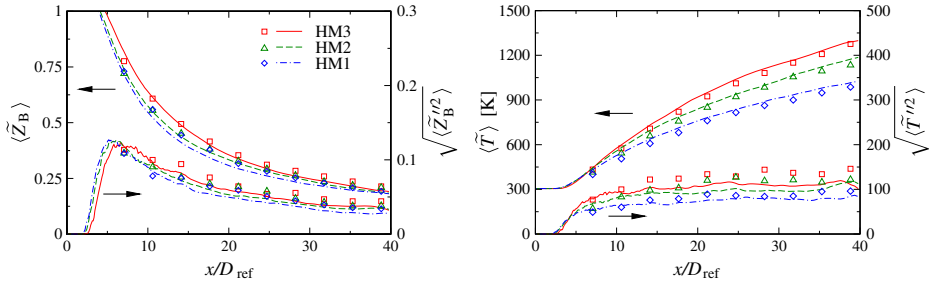

(a) Mixture Fraction (b) Temperature

Fig. 6 Comparison of computed and measured statistics along the jet centerline for **a** mixture fraction due to Bilger [20] and **b** temperature

the mean temperature in the nozzle-near region is constant in axial direction (up to $x/D_{\text{ref}} \leq 2.5$), which is a direct result of the low mixture reactivity in this region.

Centerline profiles for mean and root-mean-square (rms) quantities for mixture fraction, defined using Bilger's formulation [20], and temperature are shown in Fig. 6. Mean quantities are denoted by an angular bracket, and the resolved rms-quantity of a scalar ϕ is $\sqrt{\langle \widetilde{\phi}''^2 \rangle}$. Experimental data are shown by symbols and simulation results are given by lines. The comparison of mixture fraction profiles (Fig. 6a) shows that the agreement between simulations and experiments increases with increasing oxygen-concentration in the coflow stream, and only small deviations for the HM1-flame are evident in the middle region of the flame. The mean temperature profiles, shown in Fig. 6b, are in good agreement with experimental data, illustrating that the three-stream FPV model captures the trend of increasing oxygen-concentration on the mean flame characteristics. The comparison of rms-temperature profiles shows that $\sqrt{\langle \widetilde{T}''^2 \rangle}$ remains fairly constant and does not exceed 150K.

Radial profiles of mixture fraction are shown in Fig. 7. The simulation results are in overall good agreement with experiments, and differences are mainly confined to the region $r/D_{\text{ref}} < 2.5$, corresponding to the inner part of the coflow stream. It is also noted that the radial profiles are very similar for all three flames, and differences among these flames are mainly apparent near the jet centerline.

Radial profiles of mean temperature and mean mass fractions of H_2O, CO_2, and CO at three axial locations are shown in Fig. 8. Note that the first two measurement

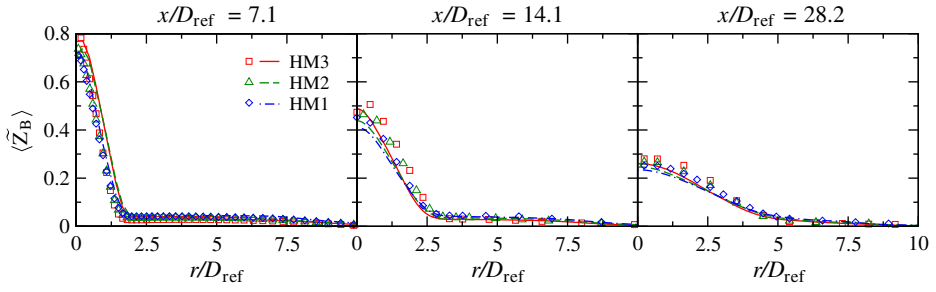

Fig. 7 Comparison of measurements (*symbols*) and computations (*lines*) for radial profiles of mean mixture fraction at three axial locations: $x/D_{\text{ref}} = 7.1$ (*left*), 14.1 (*middle*), and 28.2 (*right*)

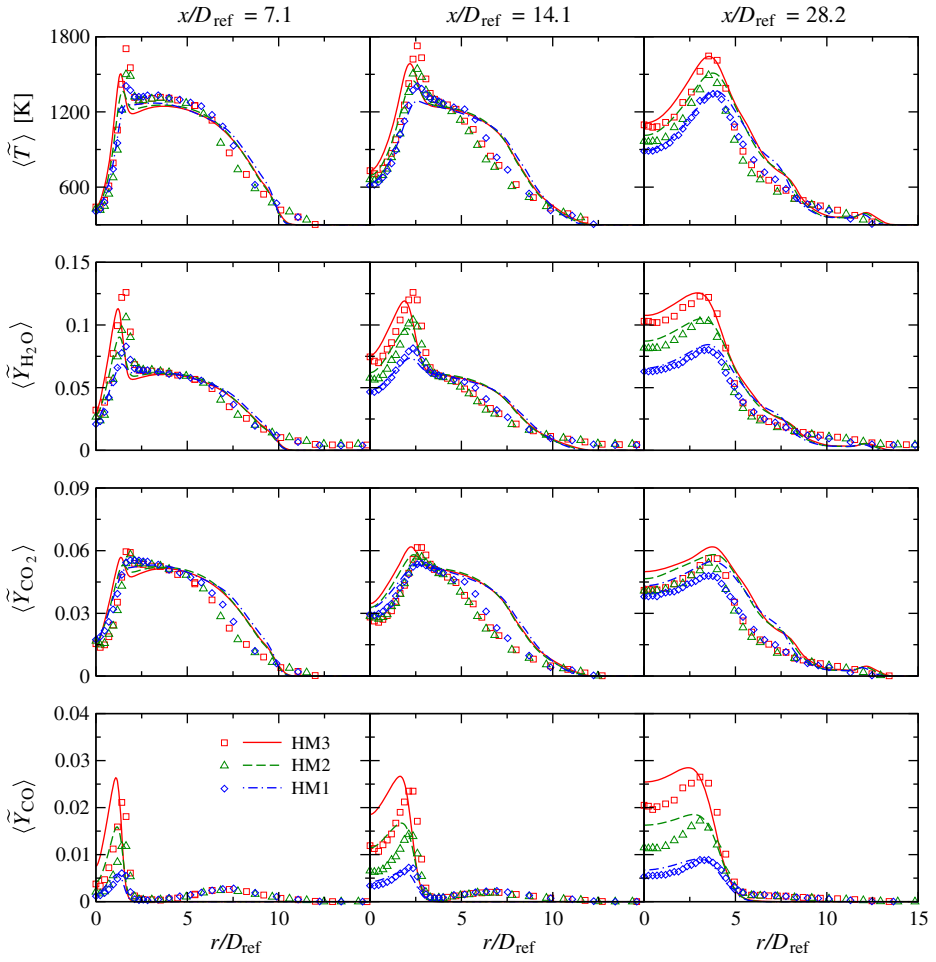

Fig. 8 Comparison of measurements (*symbols*) and computations (*lines*) for mean radial profiles of temperature and species mass fractions of H_2O, CO_2, and CO at three axial locations: $x/D_{\mathrm{ref}} = 7.1$ (*left*), 14.1 (*middle*), and 28.2 (*right*)

locations correspond to the region in which the flame is formed between the fuel-stream and the oxygen-diluted coflow. At a location above $x/D_{\mathrm{ref}} \approx 25$ the coflow is replaced by the shroud air stream, establishing the flame between the central fuel stream and the ambient air [21].

The mean temperature is shown in the first row of Fig. 8. It can be seen that the three-stream FPV model adequately captures the flame structure over this rather extended range of oxygen-dilution levels. The agreement between simulations and experiments improves with increasing downstream direction, which suggests that the simulation underestimates the reactivity of the mixture in the lower part of the flame.

The mean mass fractions of H_2O and CO_2, shown in the second and third row of Fig. 8, are in overall good agreement. The LES-FPV model captures the dependence of the major species formation on the oxygen-dilution level. It can also be seen that

discrepancies in the mixing between fuel and coflow lead to a slight shift of the flame-location towards the fuel-rich side of the flame.

Results for the carbon monoxide mass fraction are shown in the last row of Fig. 8. The predicted magnitude of the CO-emission at the peak-location is in reasonable agreement with experimental data. However, the three-stream FPV model overpredicts the CO mass fraction on the fuel-rich side of the flame. This can be attributed to the sensitivity of the CO-formation with respect to the oxidizer split on the fuel-rich side, as shown in Fig. 2b.

Mixture-fraction conditioned results are presented in Fig. 9. Note that in order to facilitate a direct comparison with measurements all quantities are conditioned on Bilger's mixture fraction formulation [20]. Conditional temperature results for all three flames are shown in the first row. Predictions for the HM3 and HM2 flames

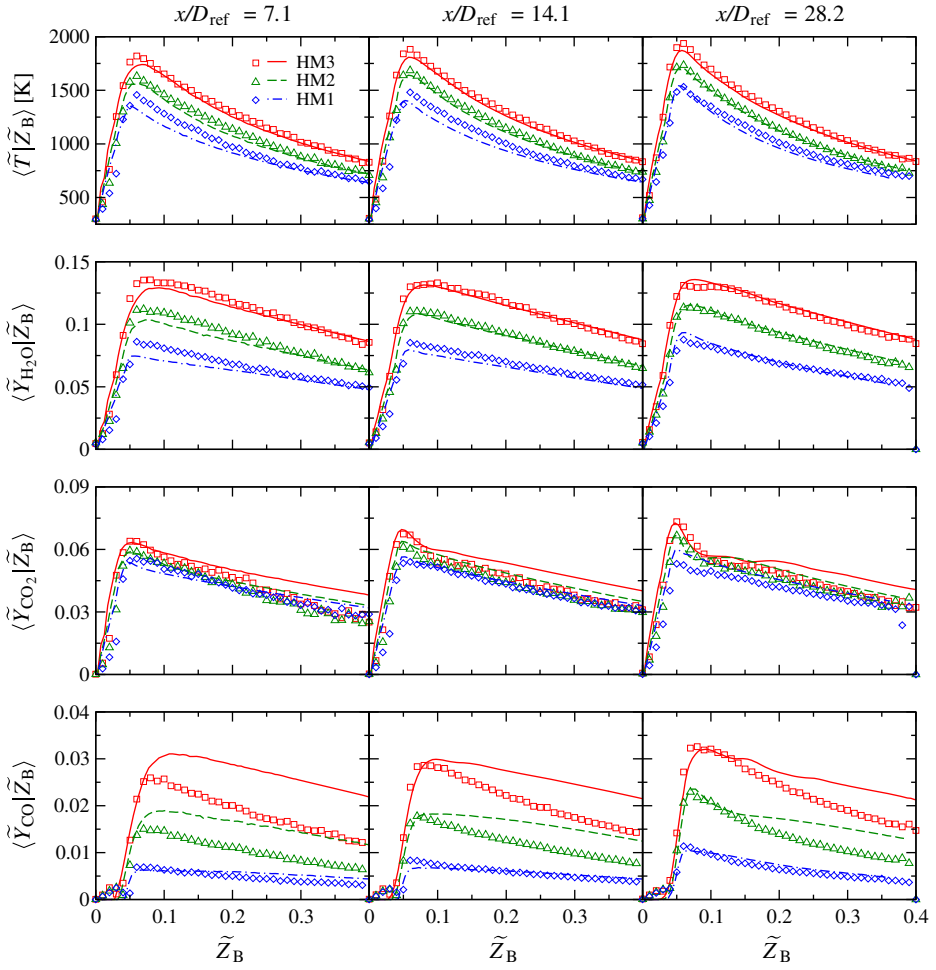

Fig. 9 Comparison of measured (*symbols*) and calculated (*lines*) conditional temperature and mass fractions of H_2O, CO_2, and CO at three axial locations: $x/D_{\mathrm{ref}} = 7.1$ (*left*), 14.1 (*middle*), and 28.2 (*right*)

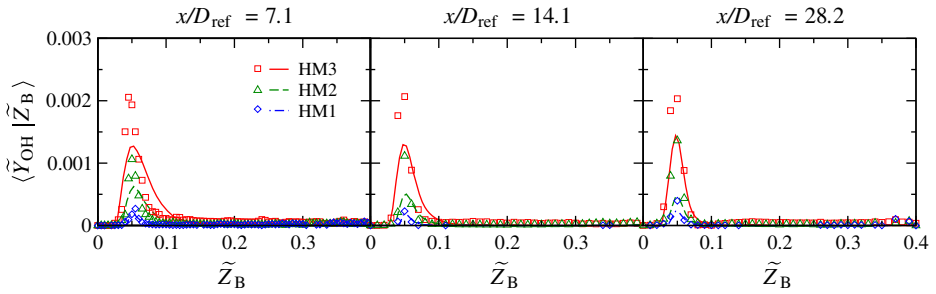

Fig. 10 Comparison of measured (*symbols*) and calculated (*lines*) conditional mass fractions of OH at three axial locations: $x/D_{\mathrm{ref}} = 7.1$ (*left*), 14.1 (*middle*), and 28.2 (*right*)

are in very good agreement with experimental data. The temperature for the HM1-configuration, having 3% O_2 in the coflow, is slightly underpredicted in the lower part of the flame. From these conditional results it can also be seen that the peak flame temperature slowly increases with increasing downstream direction for all three flames. This can be attributed to the increased oxygen-entrainment from the shroud air into the coflow.

Unlike the water mass fraction, the CO_2 results exhibit only little sensitivity to the oxygen mass fraction in the coflow-stream. The three-stream model captures the measurements for $\widetilde{Z}_{\mathrm{B}} < 0.1$, and deviations with increasing mixture fraction are apparent.

Conditional results for the CO mass fraction are presented in the last row of Fig. 9. These results further confirm the overprediction of the CO-formation on the fuel-rich side of the flame. Compared to the results for H_2O and temperature, it is interesting to note that the discrepancy between measurements and simulations increases with increasing O_2 concentration, and CO-results for the HM1 flame show the best agreement among these three flames. Further analysis showed that the main CO conversion to CO_2 is through the propagation reaction:

$$\mathrm{OH} + \mathrm{CO} \rightleftarrows \mathrm{H} + \mathrm{CO_2} \,. \tag{99}$$

As such, the good agreement of the CO_2 prediction despite the overprediction of CO might be attributed to a lower OH mass fraction, leading to a net-reduction of the CO_2-formation via reaction 99. Results for $\langle \widetilde{Y}_{\mathrm{OH}} | \widetilde{Z}_{\mathrm{B}} \rangle$ are presented in Fig. 10. Indeed, this comparison shows that the calculations underpredict the OH mass fraction for all three flames. However, it was shown in [14] that the formation of major and minor species exhibits a strong sensitivity to the scalar inflow conditions. Therefore, it is anticipated that the consideration of time-dependent scalar inflow boundary conditions could lead to further improvements of minor-species predictions [14].

5 Conclusions

Large-eddy simulations of MILD combustion in a three-stream JHC burner system were performed. The LES-approach utilizes a flamelet/progress variable model, which was extended to account for variations of the mixture composition in the oxidizer streams. This three-stream FPV model was applied to the simulation of

three flame configurations, in which the oxygen mass fraction in the coflow stream was reduced from 9% (HM3), 6% (HM2), down to 3% (HM1). In that sequence the Damköhler number decreases by more than an order of magnitude, and the peak flame temperature reduces by 450K.

Comparisons between LES results and experimental data are in overall good agreement for all three flame-configurations, demonstrating that the three-stream FPV model captures effects of increasing oxygen-dilution on the flame structure in MILD-combustion systems. Centerline profiles for temperature show an extended region over which the flame transitions between unburned and burned mixture. In this region, the magnitude of the rms-temperature fluctuations remains fairly constant and does not exceed 150K. Radial and conditional profiles for temperature and water mass fraction are well predicted by the model. Discrepancies for the carbon-containing species on the fuel-rich side are attributed to the sensitivities of the formation of CO and CO_2 to variations in the oxidizer split. The main reaction pathway for CO_2 formation is through the consumption of OH and CO via reaction 99. Due to the reduced reactivity, the formation of these intermediates is directly dependent on the inflow boundary conditions of the coflow-stream. Therefore, it is anticipated that a time-dependent description of the inflow conditions—as demonstrated in [14]—can lead to further improvements of the modeling results.

Acknowledgements This work was supported in parts through the Air Force Office of Scientific Research under Award No. FA9550-11-1-0031 and the Office of Naval Research under contract N00014-10-1-0561. JZ acknowledges financial support from the 973 Program and the LNM initial funding for young investigators.

References

1. Cavaliere, A., de Joannon M.: Mild combustion. Prog. Energy Combust. Sci. **30**, 329–366 (2004)
2. Wünning, J.A., Wünning, J.G.: Flameless oxidation to reduce thermal NO-formation. Prog. Energy Combust. Sci. **23**, 81–94 (1997)
3. Tsuji, H., Gupta, A.K., Hasegawa, T., Katsuki, M., Kishimoto, K., Morita, M.: High Temperature Air Combustion: From Energy Conservation to Pollution Reduction. CRC Press, Boca Raton (2003)
4. Katsuki, M., Hasegawa, T.: The science and technology of combustion in highly preheated air. Proc. Combust. Inst. **27**, 3135–3146 (1998)
5. Oberlack, M., Arlitt, R., Peters, N.: On stochastic Damköhler number variations in a homogeneous flow reactor. Combust. Theory Model. **4**, 495–509 (2000)
6. Plessing, T., Peters, N., Wünning, J.G.: Laseroptical investigation of highly preheated combustion with strong exhaust gas recirculation. Proc. Combust. Inst. **27**, 3197–3204 (1998)
7. Dally, B.B., Karpetis, A.N., Barlow, R.S.: Structure of turbulent non-premixed jet flames in a diluted hot coflow. Proc. Combust. Inst. **29**, 1147–1154 (2002)
8. Oldenhof, E., Tummers, M.J., van Veen, E.H., Roekaerts, D.J.E.M.: Ignition kernel formation and lift-off behavior of jet-in-hot-coflow flames. Combust. Flame **157**, 1167–1178 (2010)
9. Oldenhof, E., Tummers, M.J., van Veen, E.H., Roekaerts, D.J.E.M.: Role of entrainment in the stabilisation region of jet-in-hot-coflow flames. Combust. Flame **158**, 1553–1563 (2011)
10. Coelho, P.J., Peters, N.: Numerical simulation of a MILD combustion burner. Combust. Flame **124**(3), 503–518 (2001)
11. Christo, F.C., Dally, B.B.: Modeling turbulent reacting jets issuing into a hot and diluted coflow. Combust. Flame **142**, 117–129 (2005)
12. Kim, S.H., Huh, K.Y., Dally, B.B.: Conditional moment closure modeling of turbulent non-premixed combustion in diluted hot coflow. Proc. Combust. Inst. **30**, 751–757 (2005)

13. De, A., Oldenhof, E., Sathiah, P., Roekaerts, D.J.E.M.: Numerical simulation of Delft jet-in-hot-coflow (DJHC) flames using the eddy dissipation concept model for turbulence-chemistry interaction. Flow Turbul. Combust. **87**, 537–567 (2011)
14. Ihme, M., See, Y.C.: LES flamelet modeling of a three-stream MILD combustor: analysis of flame sensitivity to scalar inflow conditions. Proc. Combust. Inst. **33**, 1309–1317 (2010)
15. Ihme, M., Pitsch, H.: Prediction of extinction and reignition in non-premixed turbulent flames using a flamelet/progress variable model. 1. A priori study and presumed PDF closure. Combust. Flame **155**, 70–89 (2008)
16. Poinsot, T., Veynante, D.: Theoretical and Numerical Combustion. R.T. Edwards, Inc., Philadelphia (2001)
17. Ihme, M., Pitsch, H.: Prediction of extinction and reignition in non-premixed turbulent flames using a flamelet/progress variable model. 2. A posteriori study with application to Sandia flames D and E. Combust. Flame **155**, 90–107 (2008)
18. Pitsch, H.: FlameMaster v3.1: A C++ computer program for 0D combustion and 1D laminar flame calculations (1998). Available from http://www.stanford.edu/group/pitsch/
19. Bowman, C.T., Hanson, R.K., Davidson, D.F., Gardiner, W.C., Lissianski, V., Smith, G.P., Golden, D.M., Frenklach, M., Goldenberg, M.: GRI-Mech 2.11 (1997). Available from http://www.me.berkeley.edu/gri-mech/
20. Bilger, R.W., Starner, S.H., Kee, R.J.: On reduced mechanisms for methane-air combustion in nonpremixed flames. Combust. Flame **80**, 135–149 (1990)
21. Medwell, P.R., Kalt, P.A.M., Dally, B.B.: Simultaneous imaging of OH, formaldehyde, and temperature of turbulent nonpremixed jet flames in a heated and diluted coflow. Combust. Flame **148**, 48–61 (2007)